



Solid–Liquid Phase Equilibrium of the *n*-Nonane + *n*-Undecane System for Low-Temperature Thermal Energy Storage

Maria C. M. Sequeira¹ · Timur Nikitin² · Fernando J. P. Caetano^{3,4} ·
Hermínio P. Diogo¹ · João M. N. A. Fareleira¹ · Rui Fausto^{2,5}

Received: 31 May 2024 / Accepted: 16 July 2024 / Published online: 30 July 2024
© The Author(s) 2024

Abstract

The current article presents an exploration of the solid–liquid phase diagram for a binary system comprising *n*-alkanes with an odd number of carbon atoms, specifically *n*-nonane (*n*-C₉) and *n*-undecane (*n*-C₁₁). This binary system exhibits promising characteristics for application as a phase change material (PCM) in low-temperature thermal energy storage (TES), due to the fusion temperatures of the individual components, thereby motivating an in-depth investigation of the solid–liquid phase diagram of their mixtures. The *n*-nonane (*n*-C₉) + *n*-undecane (*n*-C₁₁) solid–liquid phase equilibrium study herein reported includes the construction of the phase diagram using Differential Scanning Calorimetry (DSC) data, complemented with Hot-Stage Microscopy (HSM) and low-temperature Raman Spectroscopy results. From the DSC analysis, both the temperature and the enthalpy of solid–solid and solid–liquid transitions were obtained. The binary system *n*-C₉ + *n*-C₁₁ has evidenced a congruent melting solid solution at low temperatures. In particular, the blend with a molar composition $x_{\text{undecane}} = 0.10$ shows to be a congruent melting solid solution with a melting point at 215.84 K and an enthalpy of fusion of 13.6 kJ·mol⁻¹. For this reason, this system has confirmed the initial signs to be a candidate with good potential to be applied as a PCM in low-temperature TES applications. This work aims not only to contribute to gather information on the solid–liquid phase equilibrium on the system *n*-C₉ + *n*-C₁₁, which presently are not available in the literature, but especially to obtain essential and practical information on the possibility to use this system as PCM at low temperatures. The solid–liquid phase diagram of the system *n*-C₉ + *n*-C₁₁ is being published for the first time, as far as the authors are aware.

Keywords Energy storage · Low temperature · Odd *n*-alkanes · Phase change material (PCM) · Solid–liquid phase diagram

1 Introduction

Thermal energy storage (TES), especially using phase change materials (PCM), is widely recognized as an important means to significantly contribute to solve energy problems involved in climate change. In particular, for low-temperature energy storage, the use of PCMs is emerging as a convenient approach to contribute to minimize effects tending to accelerate climate change.

Low-temperature TES can mitigate intermittency issues linked with renewable energy sources, for example, wind or solar, by storing surplus energy for use during periods of depleted generation. On the industrial field, TES systems can also present a reliable and cost-effective solution for storing excess heat generated during production for later use, enabling a balance between the existing energy supply and demand imbalances. Thus, latent heat technologies might offer a compact and feasible solution to tackle the handicap of the gap between energy supply and demand.

Many applications of PCM in cold thermal energy storage are listed in detail and commented by Gunasekara et al. [1]. The same authors stress the importance of *n*-alkanes as PCM, both pure and in blends [1], namely in eutectic systems and congruent melting solid solutions [1, 2]. However, those authors have remarked that some serious inconsistencies and disagreements have been observed, having pointed specifically the system *n*-dodecane + *n*-tridecane ($n\text{-C}_{12} + n\text{-C}_{13}$) [2]. Moreover, it is noteworthy that large-scale studies involving solid–liquid phase diagrams of *n*-alkane systems naturally do not contain a complete collection of all possible binary systems potentially suitable for low-temperature TES applications. Some of the systems with somewhat less information are, for example, some of those containing comparatively shorter alkyl chains as *n*-octane, *n*-decane, and *n*-dodecane; and, in particular, some with an odd number of carbon atoms, like *n*-nonane and *n*-undecane seem to have received comparatively less attention than the larger even ones [1, 3].

An interesting feature of pure *n*-alkanes is that the polymorphism found in the series from $n=8$ to $n=21$ has very distinct characteristics for even or odd numbered carbon atoms, according to Espeau et al. [4] and Broadhurst [5]. In particular, the *n*-alkanes with an even number of carbons show a simpler polymorphism than those with an odd number [3, 5, 6]. Moreover, for the binary short-chain *n*-alkane systems ($n < 21$), one would expect to find characteristics of the solid–liquid phase diagrams enabling some type of grouping according to the odd or even number of carbon atoms of the individual molecules involved [1, 3]. For instance, the works by Gunasekara et al. [1, 2], Espeau et al. [4], and Mondieig et al. [3] may lead to the suggestion that it is possible that a binary system with two odd alkanes would have an isomorphous congruent minimum melting solution (for example $n\text{-C}_{11} + n\text{-C}_{13}$ and $n\text{-C}_{17} + n\text{-C}_{19}$); on the other hand, a binary system with two even alkanes would possibly be expected to show an eutectic transformation (for example $n\text{-C}_8 + n\text{-C}_{10}$ and $n\text{-C}_{10} + n\text{-C}_{12}$); and finally, it could be expected that a binary mixture with one odd and one even alkanes could yield a peritectic (for example $n\text{-C}_{13} + n\text{-C}_{14}$ and $n\text{-C}_{15} + n\text{-C}_{16}$). Nevertheless, this hopeful categorization is full of exceptions from the very

start. For example, Gunasekara et al. have verified that the system $n\text{-C}_{12} + n\text{-C}_{13}$ has a congruent melting solid solution [2]. In the extensive works published by Gunasekara et al. [1] and by Mondieig et al. [3], it is in fact possible to partly observe some of this ideal grouping of solid–liquid equilibrium characteristics, but also several exceptions to it, enhancing the inherent complexity involved in these systems, especially for larger ones [1, 3]. The numerous data available evidence some irregularities and disagreement for the phase equilibrium behavior of n -alkane binary systems seeming to reinforce the idea of the complexity of these compounds [1–4]. In the light of this, it is absolutely crucial to perform complete phase equilibrium studies on n -alkane mixtures that suggest a strong potential to be used as PCM in TES applications.

The binary system $n\text{-C}_9 + n\text{-C}_{11}$ under study in the present work is particularly appropriate to be a PCM for low-temperature thermal energy storage, due to the low melting temperatures of its pure components and to the possibility to possess a congruent melting solid solution, as can be guessed on the basis of the grouping of phase diagrams described above. However, the corresponding solid–liquid phase diagram, as far as the authors are aware, has not been described in the literature yet, which is a basic information to decide on its adequacy to be a PCM for that purpose.

Thus, this study aims to contribute to decrease this lack of information by building the solid–liquid phase diagram for the system $n\text{-C}_9 + n\text{-C}_{11}$, at atmospheric pressure, using as primary information the results obtained by Differential Scanning Calorimetry (DSC), complemented by Hot Stage Microscopy (HSM) and Raman Spectroscopy data. Moreover, a particularly important information regarding application as PCM is the enthalpy of the solid–liquid phase transition, which must be tackled in this type of study and has also been done in this work.

The present work is the continuation of previous studies involving binary systems of adipates [7] and two systems of n -alkanes with an even number of carbon atoms [8], having the aim to perform a deep thermal characterization of this family of compounds and obtain useful information on the possibility to use them as PCM.

2 Experimental

2.1 Materials

In this work, $n\text{-C}_9$ and $n\text{-C}_{11}$ were used as received. The water content of the used materials was measured using a Karl-Fisher 831 KF Coulometer from Metrohm. Table 1 shows the characterization of the material samples used in this work.

Table 1 Characterization of the liquids used in this work

Name	CAS number	Supplier	Lot number	Water content (mg·kg ⁻¹)	Purity (mass fraction) (%)
n -Nonane	111-65-9	Thermo Scientific	10228094	41.5	99.3
n -undecane	1120-21-4	TCI Chemicals	XQM6G-TN	25.7	99.6

Purity as stated in the corresponding analysis certificate and water content as measured in situ

Considering the high purity of the compounds as indicated on the analysis certificates provided by the suppliers, and by the water content levels determined just before the experimental measurements, the samples were used as received.

To achieve the highest accuracy in composition, the binary mixtures for this investigation were prepared gravimetrically using a Mettler Toledo MS205DU micro balance with a precision of ± 0.01 mg.

2.2 Techniques

2.2.1 Differential Scanning Calorimetry (DSC)

The calorimetric measurements were performed with a 2920 MDSC system from TA Instruments Inc. The experimental procedure is described elsewhere [7, 8]. Thus, only a brief description is given here.

The sample masses of 4.0–9.0 mg were sealed in air inside aluminum pans and weighed with a precision of ± 0.1 μg by a Mettler UMT2 ultra-micro balance and analyzed by DSC at a scanning rate, $\beta = 5$ $\text{K}\cdot\text{min}^{-1}$ for the binary mixtures and pure compounds. Additionally, heating rates of $\beta = 1$ $\text{K}\cdot\text{min}^{-1}$ and $\beta = 2$ $\text{K}\cdot\text{min}^{-1}$ were also used in some cases, particularly for pure compounds for complementary studies (see Sects. 3.1 and S5 of the Supplementary Information). Helium (Air Liquide N55), at a flow rate of 30 $\text{cm}^3\cdot\text{min}^{-1}$, was used as purging gas. The baseline was corrected by scanning along the temperature range of the experiments using an empty pan. The temperature and heat flow scales of the instrument were calibrated at different heating rates, based on the onsets of the fusion peaks of several standards. Details of the calibration procedure are described elsewhere [9].

2.2.2 Hot Stage Microscopy (HSM)

Polarized optical microscopy observations were performed on an Olympus BX51 optical microscope. The temperature changes and stabilization were set by a Linkam LTS360 liquid nitrogen cooled cryostage and were measured with a Pt resistance thermometer. Nitrogen (Air Liquide L50), at a flow rate of 30 $\text{cm}^3\cdot\text{min}^{-1}$ was used as purging gas. The liquid samples were first placed on the glass plate, covered by a second glass and cooled down at 5 $\text{K}\cdot\text{min}^{-1}$. After solidification, the microstructure of the sample was monitored with an Olympus C5060 wide zoom camera for picture and/or movie record. Images were recorded with 250 \times magnification in the temperature range from -100 $^{\circ}\text{C}$ to 20 $^{\circ}\text{C}$ at a heat rate of 5 $\text{K}\cdot\text{min}^{-1}$.

2.2.3 Raman Spectroscopy

The Raman spectra were acquired with a Horiba LabRam HR Evolution micro-Raman system using a solid-state laser ($\lambda=532$ nm, ~ 5 mW on sample) for excitation. The samples were probed with a 50 \times objective, and the laser spot diameter on the sample was approximately 1 μm . The presented spectra were typically acquired with an acquisition time of 5 s and averaged over 10 spectra accumulations. The spectral resolution was about 5 cm^{-1} . The temperature-variation measurements were carried out with an accuracy of about 0.01 $^{\circ}\text{C}$ using the following Linkam Scientific instruments: THMS 600 stage and an LNP95 cooling system controlled by a T95-PE Linkpad controlling unit. During these measurements, optical photographs of the sample were taken using a 10 \times objective of the micro-Raman system.

3 Results and Discussion

Phase equilibrium studies for *n*-alkanes have been showing consistently the complexity, not only for the pure compounds but also for their binary mixtures [3, 10–15]. For the binary system studied in this work, *n*-C₉ and *n*-C₁₁, this is no exception. In fact, through this work several challenges related to the phase equilibrium behavior of these materials have been encountered, mainly related to the polymorphic transitions of the two pure compounds involved. According to several authors [3, 4, 12, 14, 15], both pure components, *n*-C₉ and *n*-C₁₁ present two solid phases, namely, one ordered phase, T_i, corresponding to a triclinic structure, and one rotator phase, R_i, corresponding to an orthorhombic structure.

In this investigation, three different techniques were used in order to accurately describe the phase equilibrium behavior of this binary system: DSC, hot stage microscopy (HSM), and Raman spectroscopy. In this chapter, the experimental results will be discussed and compared with information available in the literature.

3.1 Differential Scanning Calorimetry (DSC)

DSC heating curves of the pure compounds, *n*-C₉ and *n*-C₁₁ and of three of the most significant binary mixtures are presented in Fig. 1. One of the latter is a special one, as it refers to the congruent melting solid solution with a molar fraction, $x_{\text{undecane}}=0.10$.

The experimental values for temperature and enthalpy of fusion were obtained using the average values (in $\text{J}\cdot\text{g}^{-1}$), presented in Table 2, acquired from two consecutive cycles. For comparison purposes, those values were converted to $\text{kJ}\cdot\text{mol}^{-1}$ using the latest molar masses reported by IUPAC [16]. The remaining DSC heating curves for all the other studied compositions, with the corresponding temperatures and enthalpies of phase transition, are presented in the section S1 of the Supplementary Information (Fig. S1 and Table S1). The experimental *solidus* and *liquidus* temperature points were obtained from the maximum of the first and second endothermic peaks detected in the thermograms. This choice is justified by having

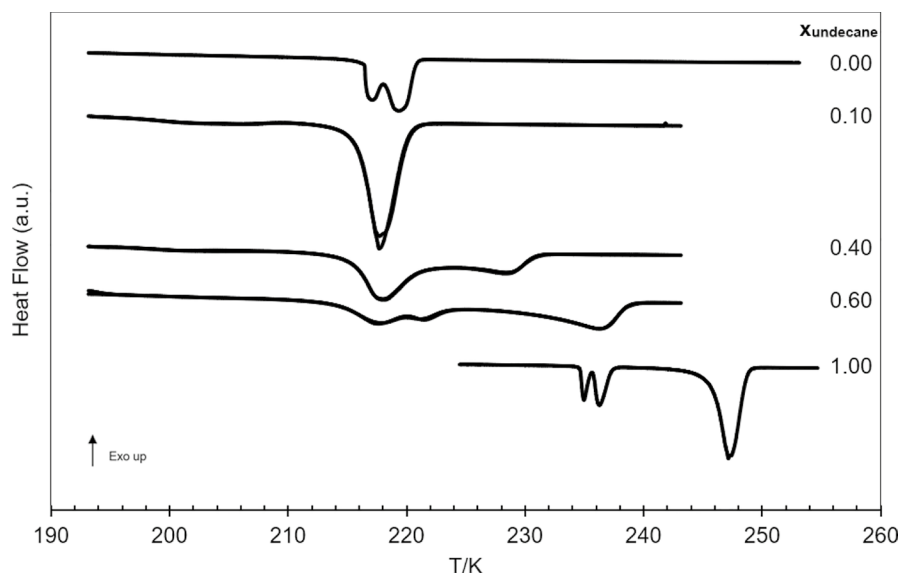


Fig. 1 DSC heating curves of n -C₉, n -C₁₁, and of some selected binary mixtures, with compositions signaled with the x_{undecane} molar fraction. The scanning rate was $\beta = 2 \text{ K}\cdot\text{min}^{-1}$ for the pure compounds and $\beta = 5 \text{ K}\cdot\text{min}^{-1}$ for the binary mixtures (exo up)

Table 2 DSC data for pure n -C₉, pure n -C₁₁, and three of their binary mixtures, including the onset temperatures, T_{onset} , maximum peak temperatures, T_{max} , and the corresponding enthalpies of fusion, $\Delta_{\text{fus}}H$, at atmospheric pressure, 0.1 MPa. The scanning rate was $\beta = 2 \text{ K}\cdot\text{min}^{-1}$ for the pure compounds and $\beta = 5 \text{ K}\cdot\text{min}^{-1}$ for the binary mixtures

x_{undecane}	DSC 1st peak			DSC 2nd peak			DSC 3rd peak		
	$T_{\text{onset}}/\text{K}$	T_{max}/K	$\Delta_{\text{fus}}H/\text{kJ}\cdot\text{mol}^{-1}$	$T_{\text{onset}}/\text{K}$	T_{max}/K	$\Delta_{\text{fus}}H/\text{kJ}\cdot\text{mol}^{-1}$	$T_{\text{onset}}/\text{K}$	T_{max}/K	$\Delta_{\text{fus}}H/\text{kJ}\cdot\text{mol}^{-1}$
0	216.46	217.12	3.8	218.28	219.34	7.4	–	–	–
0.097 ^{a)}	215.84	217.68	13.6	–	–	–	–	–	–
0.399	215.37	218.16	7.0	225.50	228.42	1.6	–	–	–
0.601	213.77 ^{b)}	217.62	6.2 ^{b)}	–	221.28	–	230.15	236.44	6.3
1	234.65	234.97	1.8	235.79	236.31	3.4	245.78	247.16	19.6

Expanded uncertainties for a 95 % confidence level ($k=2$): $U(x)=0.00007$; $U(T)=0.19 \text{ K}$; $U(\Delta_{\text{fus}}H)=8.1 \text{ J}\cdot\text{g}^{-1}$ (see Supp. Information—S4)

^{a)} Values determined with five different experiments; ^{b)} Overall T_{onset} and $\Delta_{\text{fus}}H$ value for the two overlapped peaks

binary mixtures revealing thermograms with two overlapped peaks where the onset temperatures are hardly discernible, its determination giving rise to a significant uncertainty.

In Fig. 1, it is actually possible to observe the different shapes of the curves according to the corresponding molar composition, x_{undecane} . For pure n -C₉, using

the heating rate of $5 \text{ K}\cdot\text{min}^{-1}$, two distinct, although partially overlapped, peaks upon both crystallization and melting were identified. However, it was not possible to determine accurately both the onset and maximum temperatures and the corresponding enthalpy values. Consequently, a run using a heating rate of $2 \text{ K}\cdot\text{min}^{-1}$ was conducted aiming to reveal these experimental values with enough accuracy. Consequently, the temperatures, and enthalpies of pure $n\text{-C}_9$ reported and used for the construction of the binary solid–liquid phase diagram were those determined using the rate of $2 \text{ K}\cdot\text{min}^{-1}$. Moreover, according to Espeau et al. [4], the pure $n\text{-C}_9$ may present a third peak, similarly to what happens with pure $n\text{-C}_{11}$. It is noteworthy that those authors discuss the existence of that peak as the result of a possible metastability of the compound, since they just observed this third peak upon solidification [4]. To try to corroborate this observation, a heating rate of $1 \text{ K}\cdot\text{min}^{-1}$ was further used in the DSC experiment, but no improvement in readability was obtained (see section S5 of the Supplementary Information). In fact, in the paper published by Broadhurst [5], it seems that one of the solid–solid transitions is missing for the $n\text{-C}_9$. This is indicative of the difficulties involved in phase equilibrium studies of these compounds. This difficulty, which may be an effect of impurities on the phase transition behavior of paraffins, is also stressed by Broadhurst [5]. Considering that kind of issues, it is admissible that the cause for the appearance of a third peak in the works published by Espeau et al. [4] and Mondieig et al. [3] at 218.2 K (solid – solid transition from O_i to R_i) may be related to the purity of the sample. In fact, the sample used by Espeau et al. [4] had a nominal purity slightly higher than the sample used in this work, namely 99.45% (mass), and this cannot be ruled out, in principle, as a possible contribution to the differences between those experimental results.

Continuing to analyze the thermograms shown in Fig. 1, it is noteworthy the case of pure $n\text{-C}_{11}$, whose results obtained with a heating rate of $5 \text{ K}\cdot\text{min}^{-1}$ have shown three distinct peaks, two of them overlapped. Again, aiming to determine more accurately the temperature and enthalpy values, a heating rate of $2 \text{ K}\cdot\text{min}^{-1}$ was used, which enabled to separate the two overlapped peaks. Thus, the temperatures and enthalpies reported for $n\text{-C}_{11}$ reported in this work were obtained from

Table 3 Comparison of the present T_{fus} and $\Delta_{fus}H$ experimental results, listed in Table 2, with the data reported by Espeau et al. [4] for pure $n\text{-C}_9$ and pure $n\text{-C}_{11}$, together with the corresponding absolute deviations

$n\text{-C}_9$	T_{max}/K	Dev./K	$\Delta_{fus}H/\text{kJ}\cdot\text{mol}^{-1}$	Dev./kJ·mol ⁻¹
1st peak	217.8 ± 1.1	–	–	–
2nd peak	218.2 ± 1.0	–1.08	$6.3 \pm 0.39^a)$	–2.5
3rd peak	219.5 ± 1.1	–0.16	15.0 ± 1.1	–7.6
$n\text{-C}_{11}$	T_{max}/K	Dev./K	$\Delta_{fus}H/\text{kJ}\cdot\text{mol}^{-1}$	Dev./kJ·mol ⁻¹
1st peak	236.3 ± 0.8	–1.33	0.05	1.7
2nd peak	237.4 ± 0.8	–1.09	7.0 ± 0.3	–3.6
3rd peak	247.6 ± 0.8	–0.44	22.5 ± 1.6	–2.9

^{a)} Overall enthalpy for the 1st and 2nd peaks

Table 4 Comparison of the present T_{fus} and $\Delta_{fus}H$ experimental results, listed in Table 2, with the results reported by Mondieig et al. [3] for pure n -C₉ and pure n -C₁₁, together with the corresponding absolute deviations

n -C ₉	T_{max}/K	Dev./K	$\Delta_{fus}H/kJ\cdot mol^{-1}$	Dev./ kJ·mol ⁻¹
1st peak	217.8	–	–	–
2nd peak	218.2	–1.08	6.2	–2.5
3rd peak	219.5	–0.16	15.0	–7.6
n -C ₁₁	T_{max}/K	Dev./K	$\Delta_{fus}H/kJ\cdot mol^{-1}$	Dev./ kJ·mol ⁻¹
1st peak	236.3	–1.33	0.1	1.7
2nd peak	237.4	–1.09	7.0	–3.6
3rd peak	247.6	–0.44	22.5	–2.89

Table 5 Comparison of the present T_{fus} and $\Delta_{fus}H$ experimental results, listed in Table 2, with the results reported by Broadhurst et al. [5] for pure n -C₉ and pure n -C₁₁, together with the corresponding absolute deviations

n -C ₉	T_{max}/K	Dev./K	$\Delta_{fus}H/kJ\cdot mol^{-1}$	Dev./ kJ·mol ⁻¹
1st peak	–	–	–	–
2nd peak	217.2	– 0.74	–	–
3rd peak	219.7	–0.36	6.3	1.1
n -C ₁₁	T_{max}/K	Dev./K	$\Delta_{fus}H/kJ\cdot mol^{-1}$	Dev./ kJ·mol ⁻¹
1st peak	–	–	–	–
2nd peak	236.6	– 0.29	6.9	– 3.5
3rd peak	247.6	– 0.44	22.2	– 2.6

the thermograms performed at this heating rate. Here, it is important to note that the results reported by Broadhurst [5] show two transitions only: one solid–solid and another solid–liquid. It is, therefore, possible that the purity of the samples can be in fact determinant for the phase equilibrium behavior observed for the pure compounds.

In Tables 3, 4, and 5, the absolute deviations of the temperature and enthalpy of fusion, T_{fus} and $\Delta_{fus}H$, from the literature values reported by Espeau et al. [4], Mondieig et al. [3], and Broadhurst [5] are presented for both pure components, respectively. It is possible to note that the absolute deviations of the experimental results for pure n -C₉ and n -C₁₁ presented in Tables 3 and 4 are very similar with a maximum absolute deviation for the temperature of fusion of –1.08 K for n -C₉ and –1.33 K for n -C₁₁. Regarding the enthalpy of fusion, the maximum absolute deviation is –7.6 kJ·mol⁻¹ for n -C₉ and –3.6 kJ·mol⁻¹ for n -C₁₁. Considering the results published by Broadhurst [5] in Table 5, the maximum absolute deviation for the temperature of fusion is –0.74 K for n -C₉ and –0.44 K for n -C₁₁. In the same table, it can be observed that the deviation of the present results for the enthalpy of fusion

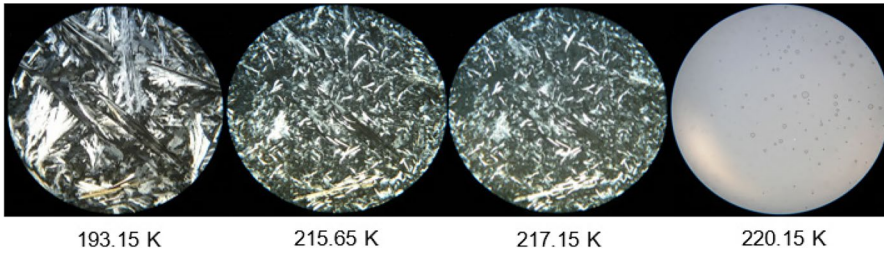


Fig. 2 HSM results for $n\text{-C}_9$ in temperature region between 193.15 K and 220.15 K, with $\times 250$ magnification

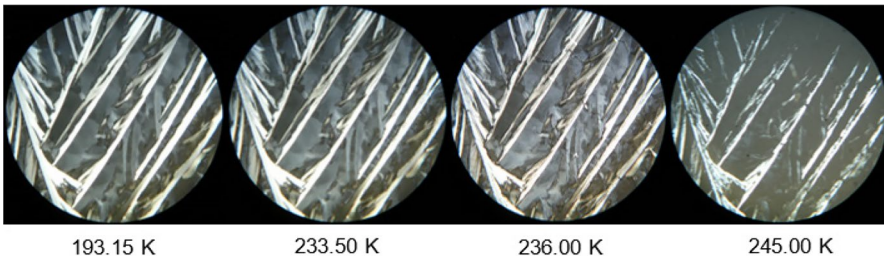


Fig. 3 HSM results for $n\text{-C}_{11}$ in temperature region between 193.15 K and 245 K, with $\times 250$ magnification

and those published by Broadhurst [5] is $1.1 \text{ kJ}\cdot\text{mol}^{-1}$ for $n\text{-C}_9$ and $-3.5 \text{ kJ}\cdot\text{mol}^{-1}$ for $n\text{-C}_{11}$, respectively. From the results presented in these tables, it can be noted that the deviations for both temperature and enthalpy of fusion are significantly lower in the case of the results published by Broadhurst [5], especially for the fusion enthalpy for $n\text{-C}_9$. In the case of the results published by Espeau et al. [4] and Mondieig et al. [3], the deviations are consistently higher, being more evident for the values of enthalpy, which can be caused by issues discussed above.

The binary mixtures for this system revealed three different types of thermograms. The binary mixture with molar fraction $x_{\text{undecane}} = 0.10$ has exhibited a single and narrow peak, which was identified as a congruent melting solid solution at 215.84 K, as supported by the complementary experimental techniques used in the present work, according to the discussion present in subsequent sections. The binary mixture with molar fraction $x_{\text{undecane}} = 0.40$ has evidenced two distinct peaks, while the one with molar fraction $x_{\text{undecane}} = 0.60$ has shown three distinct peaks. Further analysis of the binary mixtures using different heating rates in the DSC experiments (see section S5 of the Supplementary Information) and using the results from HSM and Raman spectroscopy showed that the binary mixtures presenting only two peaks also show polymorphism, even though the corresponding peak is overlapped with the two distinguishable ones.

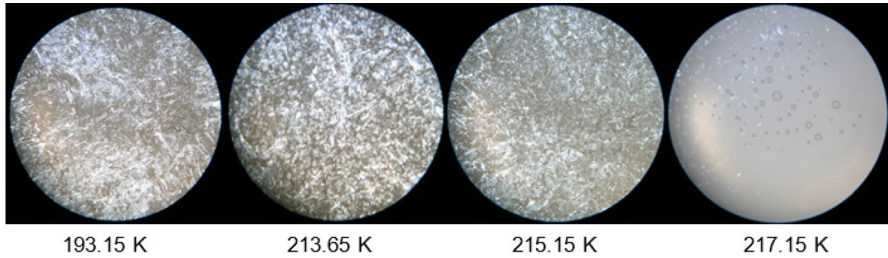


Fig. 4 HSM results for the binary mixture with molar fraction $x_{\text{undecane}}=0.10$ in temperature region between 193.15 K and 217.15 K, with $\times 250$ magnification

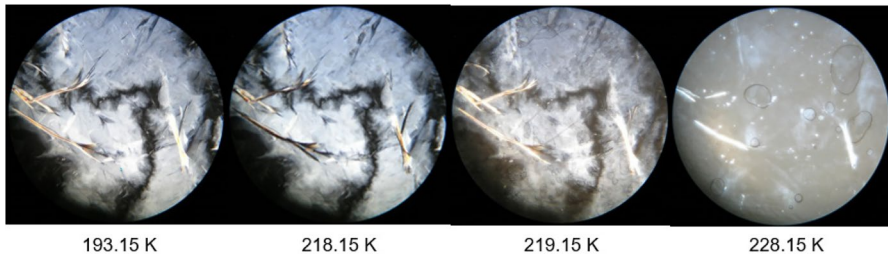


Fig. 5 HSM results for the binary mixture with molar fraction $x_{\text{undecane}}=0.40$ in temperature region between 193.15 K and 228.15 K, with $\times 250$ magnification

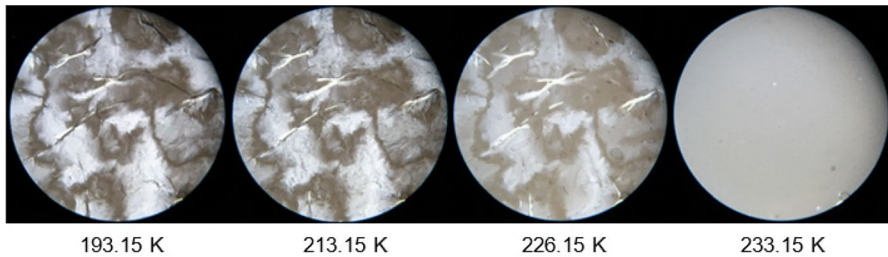


Fig. 6 HSM results for the binary mixture with molar fraction $x_{\text{undecane}}=0.60$ in temperature region between 193.15 K and 233.15 K, with $\times 400$ magnification

3.2 Hot Stage Microscopy (HSM)

Hot stage microscopy is a powerful tool to identify polymorphism [17]. In this work, it enabled us to confirm the results obtained using DSC. Using light polarization, it was possible to identify the solid–solid transitions for both pure compounds and their binary mixtures, and also, the respective solid–liquid transitions. The obtained HSM images for the pure compounds and for their most relevant binary mixtures are presented in Figs. 2, 3, 4, 5, and 6. Section S2 of the

Supplementary Information contains additional HSM images for the remaining binary mixtures and their respective analysis.

Figure 2 shows HSM images of pure $n\text{-C}_9$ together with the corresponding temperatures. In this situation, it is possible to observe, firstly, the solid–solid transition by the change of form of the solid. Secondly, at approximately 217.15 K, it is already visible the formation of some drops of liquid, and, approximately at 220.15 K, the whole sample is seen to progress into being an isotropic liquid.

In Fig. 3, the HSM images for pure $n\text{-C}_{11}$ together with the corresponding temperatures can be observed. For this compound, it was possible to identify the two solid–solid transitions, even though subtle, and the solid–liquid transitions as shown before by DSC. The solid present at 193.15 K starts to transform approximately at 233.5 K, but right after around 236 K there is a subtle change again on the form how the solid phase appears. Finally, the solid–liquid transition is visible around 245 K, revealing itself as almost instantaneous.

The most relevant HSM images for the binary mixture with molar fraction $x_{\text{undecane}}=0.10$ are represented in Fig. 4. For this binary mixture, the DSC results do not evidence the solid–solid transition, which are visible in the HSM results. This can be justified by the fact that both temperatures for solid–solid and solid–liquid transitions are very similar, thus hindering the capacity of the used DSC technique to clearly differentiate those events. The solid–liquid transition has also been revealed to be very fast, in fact, almost instantaneous, when compared to the same phase transition in the other binary mixtures with different compositions. Between 215.15 K and 217.15 K, the formation of the first drop of liquid at 215.15 K was revealed, and at 217.15 K, the sample was already completely melted. This observation, complemented with the DSC results, shows the lowest temperature of the solid–liquid phase transition, i.e., the relative minimum of both the *liquidus* and *solidus* lines, indicating that this binary mixture with a molar composition $x_{\text{undecane}}=0.10$ corresponds to a minimum congruent melting solid solution for the system $n\text{-C}_9 + n\text{-C}_{11}$.

The binary mixture with molar fraction $x_{\text{undecane}}=0.40$ was also analyzed using HSM and the corresponding results are shown in Fig. 5. For this molar fraction, it is possible to observe a very tenuous solid–solid transition only by the slight color change of the image around 219.15 K. The solid–liquid transition was also observed between 218.15 K and 228.15 K, which confirmed the DSC results.

Finally, the interpretation of the HSM results for the binary mixture with molar fraction $x_{\text{undecane}}=0.60$ raised some difficulties. Those results are displayed in Fig. 6, showing that the mixture is completely solid at 193.15 K, as expected according to the DSC results. Melting starts at approximately 213.15 K and the sample was completely liquid at 233.15 K. However, according to the DSC results, it should be possible to identify three different thermal events, namely, the beginning and the end of the melting process and, probably, polymorphism. But the DSC results alone do not provide sufficient evidence to support that claim. Using HSM, it was not possible to clearly identify the polymorphism. However, it is noteworthy that, according to the DSC results, the possible occurrence of polymorphism might be masked by the beginning of the fusion of

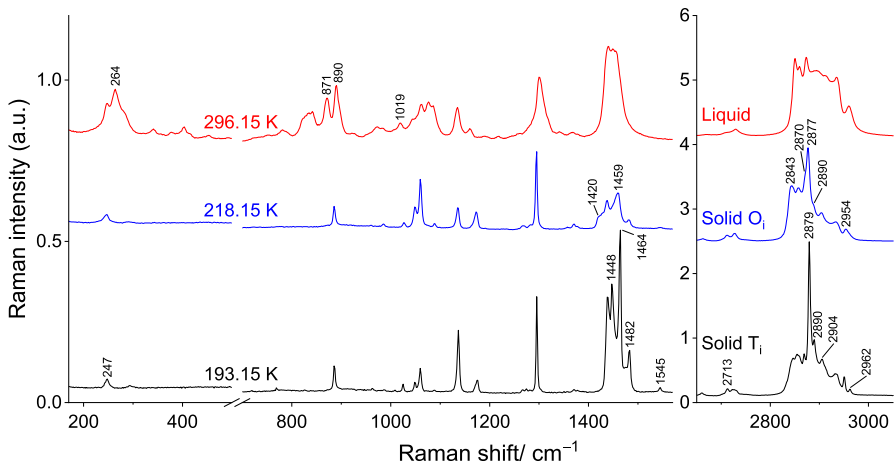


Fig. 7 Raman spectra of solid and liquid phases samples of $n\text{-C}_9$

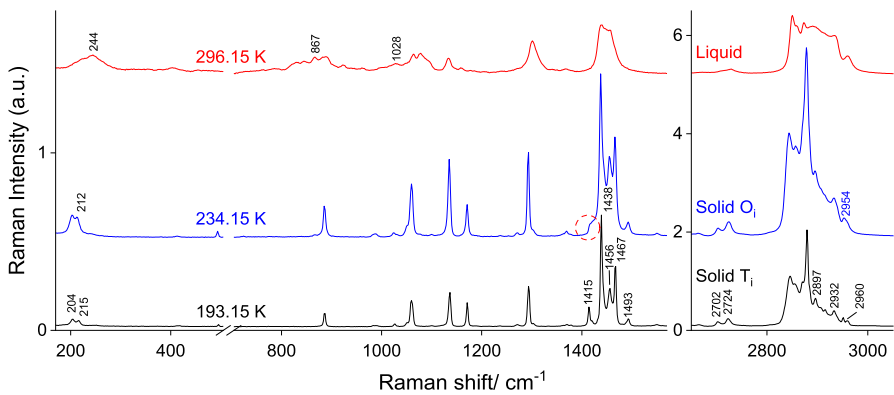


Fig. 8 Raman spectra of solid and liquid phases samples of $n\text{-C}_{11}$

the binary mixture, so that overlapping of the peaks occurs, rendering impossible to determine the enthalpy for each one of the three events independently. Because of this difficulty, the mixture with molar fraction $x_{\text{undecane}} = 0.60$ was analyzed using Raman spectroscopy with the specific purpose to try to clarify the phase transition events occurring in this temperature region for this mixture.

3.3 Raman Spectroscopy

Raman spectra were obtained for the pure compounds $n\text{-C}_9$ and $n\text{-C}_{11}$, and for the $x_{\text{undecane}} = 0.10$ (the congruent melting mixture), 0.40, and 0.60 binary mixtures at different temperatures. The experimental procedure involved initially cooling the samples to complete solidification at 193.15 K at a cooling rate of $10 \text{ K}\cdot\text{min}^{-1}$.

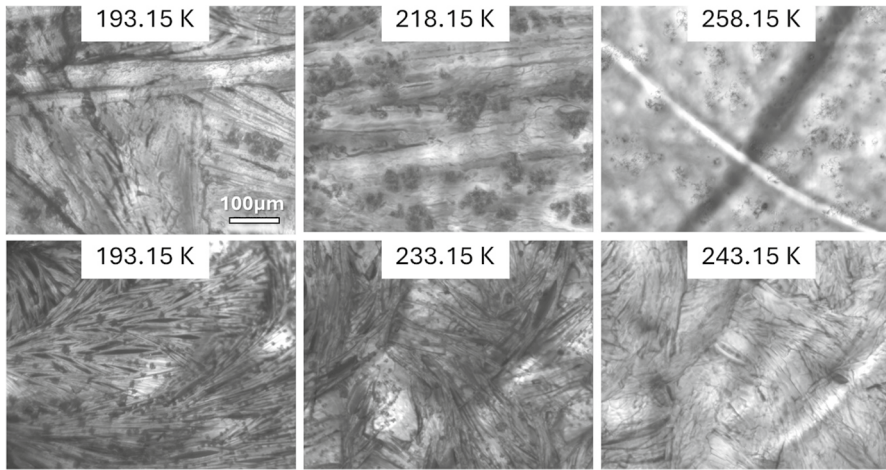


Fig. 9 Photographs of the pure $n\text{-C}_9$ (top) and $n\text{-C}_{11}$ (bottom) samples collected during the temperature-variation Raman spectroscopy experiment, with $\times 10$ magnification

Subsequently, the samples were heated at a rate of $5 \text{ K}\cdot\text{min}^{-1}$ (to allow a direct comparison of the Raman data with the DSC results) until melting, while Raman spectra were recorded at various temperatures. Additionally, optical images during the Raman experiments were taken to visually monitor the samples in real time. Raman spectra for other samples and the corresponding images are included in section S3 of the Supplementary Information.

The obtained Raman spectra for the two pure compounds account for the expected polymorphic phases of the compounds, as well as for their liquid phases (Figs. 7 and 8; Fig. 9 shows the images of the samples collected along the Raman experiments at different temperatures). The bands observed in the spectra of each phase are as follows, where the most characteristic phase-marker bands are underlined:

$n\text{-C}_9$

- Solid T_i (193.15 K): 247, 293, 885, 1048, 1173, 1295, 1438, 1448, 1464, 1483, 2713, 2869, 2879, 2889, 2904, 2950, 2962;
- Solid R_i (218.15 K): 247, 885, 1048, 1173, 1295, 1420(sh.), 1438, absence of 1447, 1459, 2712, 2843, 2870(sh.), 2877, 2887(sh.) 2904, 2954;
- Liquid (220.15 K): 247, 264, 870, 889, 1019, 1076, 1160, 1300, 1440, 1455, 2711(sh.), 2728, 2850, 2860, 2873, 2935, 2960.

$n\text{-C}_{11}$

- Solid T_i (193.15 K): 204, 215, 1027, 1048 (sh.), 1060, 1136, 1172, 1295, 1379, 1416, 1438, 1456, 1466, 1493, 2703, 2724, 2896, 2907, 2916, 2950, 2960;
- Solid R_i/O_i (234.15 K): 204, 212, 885, 1027, 1048 (sh.), 1060, 1136, 1172, 1295, 1369 1438, 1456, 1466, 1492, 2702, 2724, 2870, 2896, 2907, 2954;

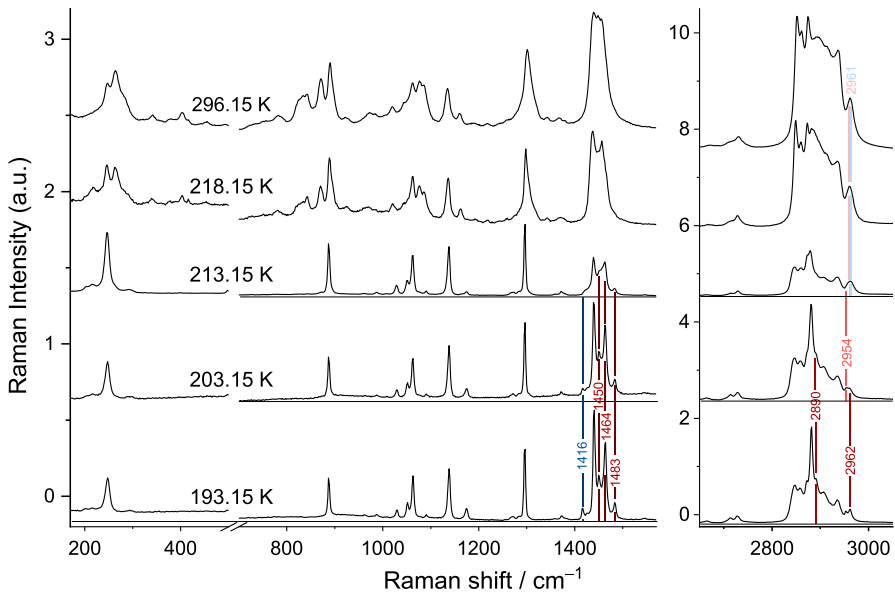


Fig. 10 Temperature-variation Raman spectra for the binary mixture $x_{\text{undecane}}=0.10$. The vertical colored lines and band positions serve as guides to indicate the most important transformations in the spectra. The red color corresponds to C9, while the blue color corresponds to C11. The darkest colors indicate Ti solid phases, lighter colors denote Ri solid phases, and the lightest colors represent the liquid phases (Color figure online)

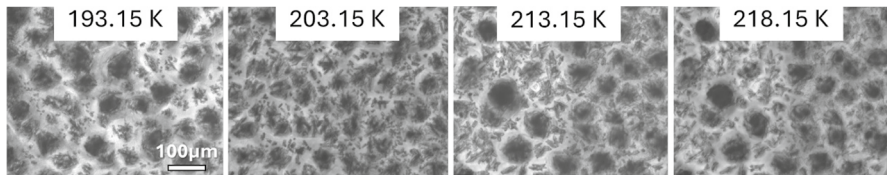


Fig. 11 Photographs of the $x_{\text{undecane}}=0.10$ sample, collected during the temperature-variation Raman spectroscopy experiment, with $\times 10$ magnification

- Liquid (247.15 K): [244](#), [829](#), [847](#), [866](#), [1064](#), [1078](#), [1301](#), [1440–1456](#), [2711–2730](#), [2851](#), [2874](#), [2960](#).

For the $x_{\text{undecane}}=0.10$ sample (Fig. 10; see also Fig. 11 for the photographs of the sample taken during the experiment), at 193.15 K, the spectrum shows the marker bands for the T_i solid phases of $n\text{-C}_9$ at 1450 cm^{-1} , 1464 cm^{-1} , 1483 cm^{-1} , 2890 cm^{-1} , and 2962 cm^{-1} , and of $n\text{-C}_{11}$ at 1416 cm^{-1} . At 203.15 K, the marker bands at 2890 cm^{-1} and 2962 cm^{-1} disappeared, and the marker band at 2954 cm^{-1} appeared, meaning that the transition from the $n\text{-C}_9$ T_i solid phase to the R_i occurred. At 213.15 K, the R_i marker band at 2954 cm^{-1} is already visible, while the T_i marker band at 1450 cm^{-1} is almost invisible. The absence of the band at 1416 cm^{-1} is a characteristic feature for the R_i solid phase. Simultaneously, the marker band at 2960 cm^{-1} makes its first appearance, which is characteristic

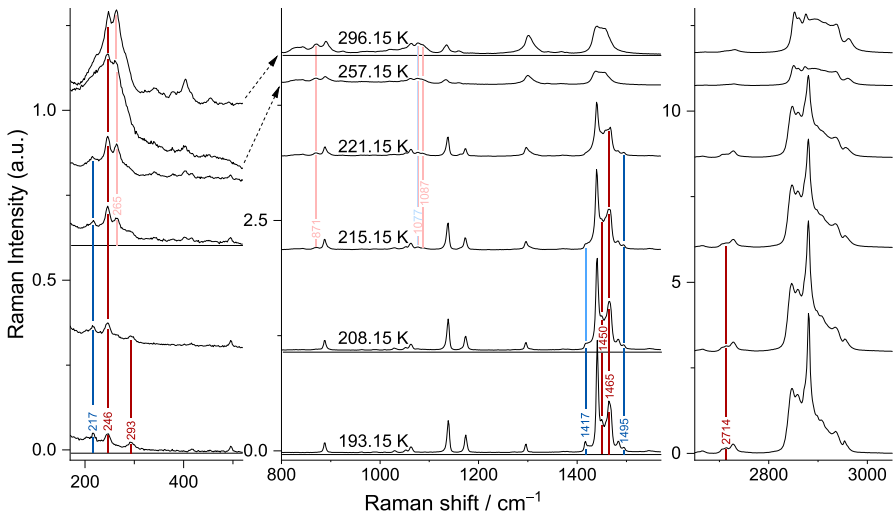


Fig. 12 Temperature-variation Raman spectra for the binary mixture $x_{\text{undecane}}=0.40$. The vertical colored lines and band positions serve as guides to indicate the most important transformations in the spectra. The red color corresponds to C9, while the blue color corresponds to C11. The darkest colors indicate Ti solid phases, lighter colors denote Ri solid phases, and the lightest colors represent the liquid phases (Color figure online)

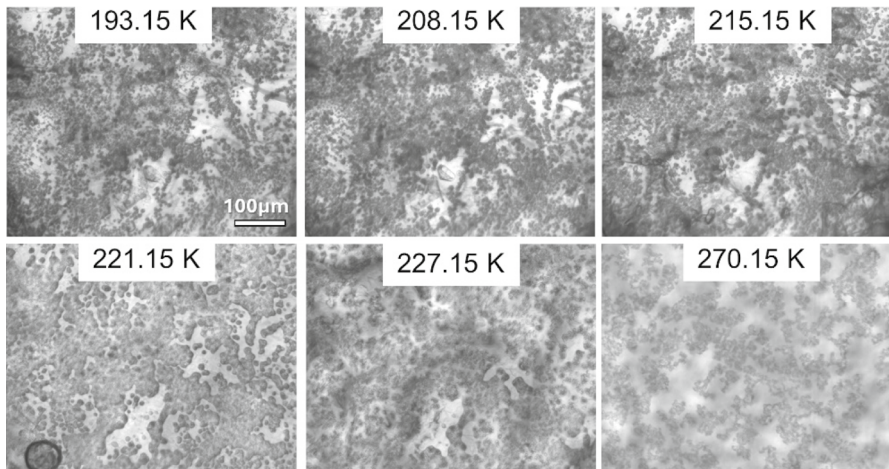


Fig. 13 Photographs of the $x_{\text{undecane}}=0.40$ sample, collected during the temperature-variation Raman spectroscopy experiment, with $\times 10$ magnification

for both compounds in the liquid state. At 218.15 K, as expected, the sample is already in the liquid state, and the spectrum shows the marker bands at 264, 1160, and 2859 cm^{-1} for $n\text{-C}_9$ and those at 2873, 2850, and 2960 cm^{-1} for both $n\text{-C}_9$ and $n\text{-C}_{11}$. The Raman experiments also showed that the melting for this sample

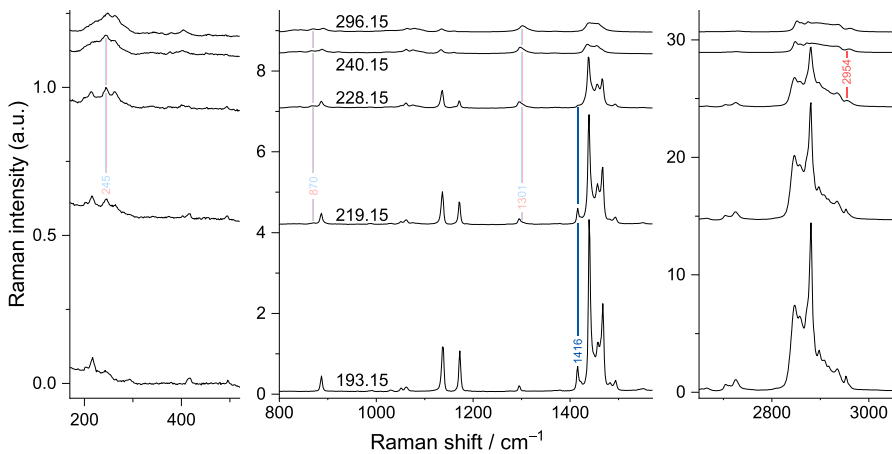


Fig. 14 Temperature-variation Raman spectra for the binary mixture $x_{\text{undecane}}=0.60$. The vertical colored lines and band positions serve as guides to indicate the most important transformations in the spectra. The red color corresponds to C9, while the blue color corresponds to C11. The darkest colors indicate Ti solid phases, lighter colors denote Ri solid phases, and the lightest colors represent the liquid phases (Color figure online)

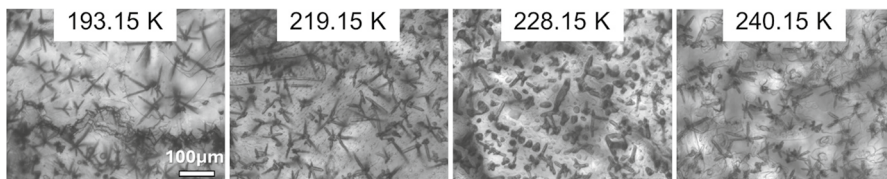


Fig. 15 Photographs of the $x_{\text{undecane}}=0.60$ sample, collected during the temperature-variation Raman spectroscopy experiment, with $\times 10$ magnification

is almost instantaneous, reinforcing the fact that this is a congruent melting solid solution.

In the case of the $x_{\text{undecane}}=0.40$ sample (Figs. 12 and 13), at 193.15 K, the spectrum evidences the marker bands for the T_i solid phase of $n\text{-C}_9$ at 246, 293, 1450, 1465, and 2714 cm^{-1} and of $n\text{-C}_{11}$ at 217, 1417, and 1495 cm^{-1} . At 208.15 K, the polymorphic changes can already be observed as evidenced by the notable decrease of the marker band at 1417 cm^{-1} . By 215.15 K, the spectra reveal some bands associated with a liquid phase, namely, the marker bands at 265, 871, and 1087 cm^{-1} for the liquid phase of $n\text{-C}_9$ and the band at 1077 cm^{-1} specific for the liquid phases of both $n\text{-C}_9$ and $n\text{-C}_{11}$. This observation proves that both compounds start to melt at the same time, which is characteristic for a solid solution. At 221.15 K, it is possible to observe the transformation of the marker band 1416 cm^{-1} for the $n\text{-C}_{11}$ T_i solid form to the one characteristic for the R_i at 1369 cm^{-1} . Only at 257.15 K, it is possible to say that the sample is completely liquid, the spectrum not showing any marker band for the solid phases.

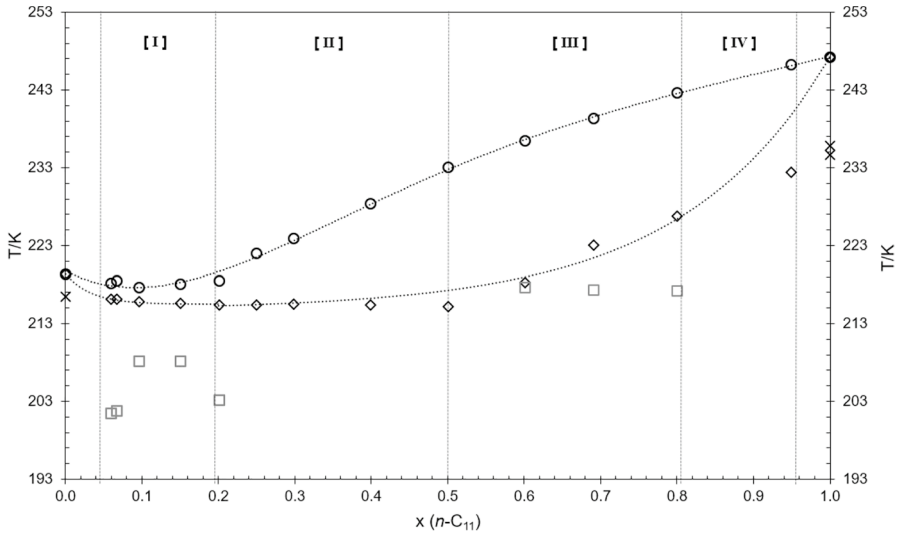


Fig. 16 Proposed binary solid–liquid phase diagram of $n\text{-C}_9$ and $n\text{-C}_{11}$; \cdots liquidus and solidus lines, \circ experimental liquidus data points, \diamond experimental solidus data points, \square solid–solid transitions for binary mixtures, \times solid–solid transitions for pure $n\text{-C}_9$ and $n\text{-C}_{11}$

For the $x_{\text{undecane}} = 0.60$ sample (Figs. 14 and 15), the Raman spectrum of the mixture at 193.15 K represents a superposition of those for the $n\text{-C}_9$ and $n\text{-C}_{11}$ T_i solid phases. At 219.15 K, it is already possible to identify the marker bands (with a very low intensity) for the $n\text{-C}_9$ and $n\text{-C}_{11}$ liquid phases at 245 cm^{-1} , 870 cm^{-1} , 1076 cm^{-1} , and a shoulder at 1301 cm^{-1} . At 228.15 K, it is possible to see changes in the spectrum related to the polymorphic transitions for both $n\text{-C}_9$, with the appearance of the marker broad band at 2954 cm^{-1} characteristic for the R_1 solid phase, and $n\text{-C}_{11}$, with the almost total disappearance of the marker band at 1416 cm^{-1} characteristic for the T_i solid phase. At 240.15 K, the Raman spectrum is closely similar to that of the sample obtained at room temperature indicating that the mixture transformed to the liquid state.

3.4 Solid–Liquid Binary Phase Diagram

The construction of the solid–liquid binary phase diagram was based on the onset temperatures, T_{onset} , obtained using the DSC technique, as shown in Fig. 16. The onset temperatures were used instead of the maximum peak temperatures for the solidus line, as it has been done in previous works [7, 8], after a careful analysis of the results using both onset and maximum temperature values. The argument used in those previous works for the use of the maximum values was based on the fact that, in binary mixtures, overlapping of two or more peaks often occurs, which prevents the accurate determination of the T_{onset} values. For the present system, however, that overlapping was observed for one binary mixture only, and therefore, upon evaluation of the obtained DSC results, use of the onset values for the construction of the

binary phase diagram was preferred. This choice has been thought to provide an easier definition of a suitable *solidus* line for the *n*-C₉ rich side of the diagram—where the congruent melting solid solution is located ($x_{\text{undecane}}=0.10$)—as discussed in section S6 of the Supplementary Information. Nevertheless, values of both the T_{onset} and T_{max} are given in Tables 2 and S1 for all compositions of the studied binary mixtures and for the pure compounds. Additionally, the results from HSM and Raman spectroscopy were used to corroborate and/or complete the DSC results enabling the identification of the different regions of the phase diagram.

For the binary system under study, polymorphic events are widely present, and thus, HSM and Raman spectroscopy techniques have been very important to describe those events. Polymorphic events shown some difficulty of interpretation using DSC alone, since it is not possible to assign the peaks to a specific event without resort to an independent method, for instance, HSM or Raman spectroscopy. In fact, after careful treatment of the results using the three different techniques, it was possible to define four distinct regions (I, II, III, and IV) in the phase diagram, in accordance with the available results.

The region [I] involves the samples with molar fractions $0.06 \leq x_{\text{undecane}} \leq 0.20$, which showed polymorphism in the 203 K–213 K region, as depicted in Fig. 16. This behavior was first observed with DSC, although the corresponding peaks were very smooth. In this case, it was necessary to resort to independent means that could unequivocally assign it to a polymorphic effect. However, upon the analysis using HSM the doubts remained, as no explicit evidence of polymorphism could be observed. Only upon a careful Raman analysis, it was possible to confirm the polymorphic transition for these mixtures in the temperature window 203 K–213 K.

The region [II] includes the binary mixtures with molar fractions $0.20 < x_{\text{undecane}} < 0.50$, which originated two single peaks in the DSC thermograms. However, HSM and Raman spectroscopy revealed a polymorphic transition occurring simultaneously with the solid–liquid transition. That is, once the beginning of the solid–liquid transition has occurred, as indicated by the appearance of the first peak (lowest T), and before its end, evidenced by the second peak (highest T), the remaining solid phase goes through a solid–solid transition. This event should correspond to a second peak (mid T), which, however, could not be detected.

The region [III] includes the mixtures with molar fractions $0.50 < x_{\text{undecane}} \leq 0.80$, which produced three distinct peaks in the DSC results. In these cases, we have tried to assign the corresponding solid–liquid transition and the solid–solid transition peaks. Using the HSM and the Raman spectroscopy, it was possible to realize that the solid–solid transition appears in the first peak (lowest T). Afterward, at higher temperatures, two other peaks show up, corresponding to the beginning (mid T) and the end of the solid–liquid transition (highest T).

Considering what was described for the samples of regions [II] and [III], the mixture with $x_{\text{undecane}} = 0.50$ seems to be a turning point, because using Raman spectroscopy, it was shown that the polymorphic transition begins simultaneously with the solid–liquid transition. Moreover, aiming to clarify the DSC results, particularly for this binary mixture, a study with a lower heating rate was performed (see section S5 in the Supplementary Information), which reinforced the conclusion that this mixture was indeed the turning point for the sequence of those phase equilibrium events.

Finally, the samples included in region [IV] with molar fractions $0.80 < x_{\text{undecane}} \leq 0.95$ have demonstrated no polymorphic transitions in the studied temperature region.

As the main aim of the present work is to determine the suitability of the system $n\text{-C}_9 + n\text{-C}_{11}$ to be used as a low-temperature PCM, the most important part of the phase diagram is the existence of a congruent melting solid solution with composition $x_{\text{undecane}} = 0.10$. Nevertheless, it should be remarked that attention to the solid–liquid equilibrium along the whole composition range is necessary to substantiate that claim. That justifies the attention given to the solid–solid, and not just the solid–liquid, transitions discussed above.

4 Conclusions

Paraffins have been extensively identified as potential PCMs for thermal energy storage due to their advantages over other systems, such as being chemically inert, non-corrosive, odorless, low cost, and nontoxic. However, for low-temperature applications, only a few n -alkanes systems have been studied, particularly those with odd alkyl chains. In the present work, the binary system involving the odd n -alkanes, $n\text{-C}_9$ and $n\text{-C}_{11}$, was studied to investigate their ability to be used for low-temperature energy storage applications, addressing the lack of research on the use of alkanes as PCMs for cold-energy storage.

From the DSC analysis and Raman spectroscopy with temperature-variation results for thirteen binary mixtures with different molar fractions and the two pure components, the temperature and the enthalpy of solid–liquid and solid–solid transitions were obtained. Hot stage polarization microscopy was used to visually and semi-quantitatively complement some thermal events evidenced by DSC, namely, solid–liquid and solid–solid (polymorphic) phase transitions. This binary system has shown a congruent melting solid solution at low temperatures, namely, the blend with a molar composition $x_{\text{undecane}} = 0.10$ with a melting point of 215.84 K and an enthalpy of fusion of $13.6 \text{ kJ}\cdot\text{mol}^{-1}$. In this context, the present binary system confirms to have appropriate characteristics for thermal energy storage applications at sub-zero temperatures, based on its phase equilibrium behavior and the appreciably high energy storage performance, considering its latent heat of fusion for this temperature region.

To the best of the authors' knowledge, the solid–liquid phase diagram of the $n\text{-C}_9 + n\text{-C}_{11}$ system has not previously been published in the specialized literature. Therefore, the current results create an avenue for evaluating other thermophysical properties such as thermal conductivity studies that are required for its valuable practical application as a PCM.

Supplementary Information The online version contains supplementary material available at <https://doi.org/10.1007/s10765-024-03411-6>.

Author Contributions MCMS participated in all the work, its execution, and interpretation. TN and RF participated in the Raman spectra and interpretation. HPD participated in the DSC and interpretation.

FJPC, JMNAF, and HPD participated in the organization of the experimental work and interpretation of the results. All authors participated in the writing of this paper.

Funding Open access funding provided by FCTIFCCN (b-on). This work was supported by Fundação para a Ciência e a Tecnologia (FCT), Portugal, Projects UIDB/00100/2020 (<https://doi.org/10.54499/UIDB/00100/2020>), UIDP/00100/2020 (<https://doi.org/10.54499/UIDP/00100/2020>), UIDB/00313/2020 (<https://doi.org/10.54499/UIDB/00313/2020>), UIDP/00313/2020 (<https://doi.org/10.54499/UIDP/00313/2020>), and IMS—LA/P/0056/2020UIDB/00100/2020 (<https://doi.org/10.54499/LA/P/0056/2020>). M.C.M. Sequeira acknowledges the PhD grant funded by FCT ref. UI/BD/152239/2021 (<https://doi.org/10.54499/UI/BD/152239/2021>).

Data Availability Data will be made available on request. No datasets were generated or analyzed during the current study.

Declarations

Competing interests The authors declare that they have no competing financial interest or personal relationships that could have appeared to influence the work reported in this paper. The authors declare no competing interests.

Open Access This article is licensed under a Creative Commons Attribution 4.0 International License, which permits use, sharing, adaptation, distribution and reproduction in any medium or format, as long as you give appropriate credit to the original author(s) and the source, provide a link to the Creative Commons licence, and indicate if changes were made. The images or other third party material in this article are included in the article's Creative Commons licence, unless indicated otherwise in a credit line to the material. If material is not included in the article's Creative Commons licence and your intended use is not permitted by statutory regulation or exceeds the permitted use, you will need to obtain permission directly from the copyright holder. To view a copy of this licence, visit <http://creativecommons.org/licenses/by/4.0/>.

References

1. S.N. Gunasekara, V. Martin, J.N. Chiu, Phase equilibrium in the design of phase change materials for thermal energy storage: state-of-the-art. *Renew. Sustain. Energy Rev.* **73**, 558–581 (2017). <https://doi.org/10.1016/j.rser.2017.01.108>
2. S.N. Gunasekara, S. Kumova, J.N.W. Chiu, V. Martin, Diagramme de phase expérimental du système dodécane–tridécanne comme matériau à changement de phase pour des applications d'entreposage frigorifique. *Int. J. Refrig.* **82**, 130–140 (2017). <https://doi.org/10.1016/j.ijrefrig.2017.06.003>
3. D. Mondieig, F. Rajabalee, V. Metivaud, H.A.J. Oonk, M.A. Cuevas-Diarte, n-Alkane binary molecular alloys. *Chem. Mater.* **16**, 786–798 (2004). <https://doi.org/10.1021/cm031169p>
4. H.A.J. Espeau, P. Roblès, L. Mondieig, D. Haget, Y. Cuevas-Diarte, M.A. Oonk, Mise au point sur le comportement énergétique et cristallographique des n-alcane I. Série de C₈H₁₈ à C₂₁H₄₄. *J. Chim. Phys.* **93**, 1217–1238 (1996). <https://doi.org/10.1051/jcp/1996931217>
5. M.G. Broadhurst, An analysis of the solid phase behavior of the normal paraffins. *J. Res.* **66A**, 241–249 (1962). <https://doi.org/10.6028/jres.066A.024>
6. P. Espeau, L. Robles, M.A. Cuevas-Diarte, D. Mondieig, Y. Haget, Thermal cycling of molecular alloys and eutectics containing alkanes for energy storage. *Mater. Res. Bull.* **31**, 1219–1232 (1996). [https://doi.org/10.1016/0025-5408\(96\)00123-7](https://doi.org/10.1016/0025-5408(96)00123-7)
7. M.C.M. Sequeira, B.A. Nogueira, F.J.P. Caetano, H.P. Diogo, J.M.N.A. Fareleira, R. Fausto, Di-alkyl adipates as new phase change material for low temperature energy storage. *Int. J. Thermophys.* (2023). <https://doi.org/10.1007/s10765-023-03274-3>
8. M.C.M. Sequeira, B.A. Nogueira, F.J.P. Caetano, H.P. Diogo, J.M.N.A. Fareleira, R. Fausto, Solid-liquid phase equilibrium: alkane systems for low-temperature energy storage. *Int. J. Thermophys.* **45**, 1–22 (2024). <https://doi.org/10.1007/s10765-023-03317-9>

9. J.J. Moura Ramos, R. Taveira-Marques, H.P. Diogo, Estimation of the fragility index of indomethacin by DSC using the heating and cooling rate dependency of the glass transition. *J. Pharm. Sci.* **93**, 1503–1507 (2004). <https://doi.org/10.1002/jps.20061>
10. L. Ventolà, T. Calvet, M.Á. Cuevas-Diarte, V. Métivaud, D. Mondieig, H. Oonk, From concept to application. A new phase change material for thermal protection at -11 °C. *Mater. Res. Innov.* **6**, 284–290 (2002). <https://doi.org/10.1007/s10019-002-0213-3>
11. D. Mondieig, P. Espeau, L. Robles, Y. Haget, H.A.J. Oonk, M.A. Cuevas-Diarte, Mixed crystals of n-alkane pairs: a global view of the thermodynamic melting properties. *J. Chem. Soc. Faraday Trans.* **93**, 3343–3346 (1997). <https://doi.org/10.1039/a703255b>
12. H.E. King, E.B. Sirota, H. Shao, D.M. Singer, A synchrotron x-ray scattering study of the rotator phases of the normal alkanes. *J. Phys. D Appl. Phys.* **26**, 8–136 (1993). <https://doi.org/10.1088/0022-3727/26/8B/021>
13. H.A.J. Oonk, D. Mondieig, Y. Haget, M.A. Cuevas-Diarte, perfect families of mixed crystals: the rotator I N-alkane case. *J. Chem. Phys.* **108**, 715–722 (1998). <https://doi.org/10.1063/1.475431>
14. F. Rajabalee, V. Métivaud, D. Mondieig, Y. Haget, M.A. Cuevas-Diarte, New insights on the crystalline forms in binary systems of n-alkanes: characterization of the solid ordered phases in the phase diagram tricosane + pentacosane. *J. Mater. Res.* **14**, 2644–2654 (1999). <https://doi.org/10.1557/JMR.1999.0354>
15. F. Rajabalee, P. Negrier, D. Mondieig, M.A. Cuevas-Diarte, Ordered phases in n-heptacosane (C₂₇H₅₆) Structure determination of the Mdc1 phase. *Chem. Mater.* **14**, 4081–4087 (2002). <https://doi.org/10.1021/cm021118c>
16. T. Prohaska et al., Standard atomic weights of the elements 2021 (IUPAC technical report). *Pure Appl. Chem.* **94**, 573–600 (2022). <https://doi.org/10.1515/pac-2019-0603>
17. D.R. Hilfiker, *Polymorphism in the Pharmaceutical Industry* (Wiley-VCH, Weinheim, 2006)

Publisher's Note Springer Nature remains neutral with regard to jurisdictional claims in published maps and institutional affiliations.

Authors and Affiliations

Maria C. M. Sequeira¹  · Timur Nikitin²  · Fernando J. P. Caetano^{3,4}  ·
Hermínio P. Diogo¹  · João M. N. A. Fareleira¹  · Rui Fausto^{2,5} 

✉ Fernando J. P. Caetano
fernando.caetano@uab.pt

✉ Hermínio P. Diogo
hdiogo@tecnico.ulisboa.pt

¹ Centro de Química Estrutural, Institute of Molecular Sciences, Departamento de Engenharia Química, Instituto Superior Técnico, Universidade de Lisboa, Av. Rovisco Pais, 1049-001 Lisbon, Portugal

² CQC-IMS, Departamento de Química, Universidade de Coimbra, 3004-535 Coimbra, Portugal

³ Departamento de Ciências e Tecnologia, Universidade Aberta, 1269-001 Lisbon, Portugal

⁴ Centro de Química Estrutural, Institute of Molecular Sciences, Instituto Superior Técnico, Universidade de Lisboa, Av. Rovisco Pais, 1049-001 Lisbon, Portugal

⁵ Department of Physics, Faculty of Sciences and Letters, Istanbul Kultur University, Ataköy Campus, Bakirköy, 34156 Istanbul, Turkey